Estimation Method for Statistical Eye Diagram in a Nonlinear Digital Channel

Chiu-Chih Chou, *Student Member, IEEE*, Sheng-Yun Hsu, and Tzong-Lin Wu, *Fellow, IEEE*

***Abstract*—An estimation method for statistical eye diagram in a digital channel with nonlinear circuitry is proposed, which is based on the superposition of multiple bit pattern responses method. The proposed method captures the nonlinear effects in the channel by using 2^m bit pattern responses as bases for doing superposition. By selecting a larger *m*, the nonlinear performance of the channel can be captured more accurately. Besides the statistical eye diagram, a corresponding bathtub curve computing method is also proposed, which not only gives the total bit error rate (BER) distribution, but also the BER when transmitting a logic "1" signal and the BER of transmitting "0." The proposed method is verified using two different channel topologies: the push–pull output driver and the open-drain output driver. The predicted results are in agreement with the result of PRBS, while the CPU time of this method is much less than PRBS.**

***Index Terms*—Bit error rate (BER), channel evaluation, eye diagram prediction, nonlinear driver, probability density function, signal integrity.**

I. Introduction

VARIOUS methodologies for fast and accurate signal integrity (SI) estimation have been proposed [1]–[19] to serve as substitutes for the time-consuming pseudorandom bit sequence (PRBS) simulation. One category of these methods uses superposition approach [2]–[9], in which the received waveform of PRBS at receiver is constructed, approximately, by using superposition of some basis waveforms. Instead of directly running the lengthy PRBS simulation, one only needs to run circuit simulation for a relatively short period of time just to obtain the received waveforms of those bases. Casper *et al.* [2] take the single-bit response (SBR) as the only basis waveform for superposition. The SBR is the received waveform of the input pattern "010." Using SBR is equivalent to use the step response alone, as investigated in [3]. If the output driver has mismatched pull-up and pull-down transistors, then two step responses, one being the "rising response" or the "01" response and the other the "falling response" or the "10" response, are needed as basis waveforms for superposition in order to have accurate prediction, as developed in [4].

If the circuits are significantly nonlinear, there will be error using SBR or double step responses methods [4], [5]. For example, when the output driver switches between 0 and 1, currents flow through the power distribution network (PDN) and causes V_{DD} to be perturbed. Before such transient ripples become stable, the output driver will respond differently to the new incoming signals because of the time-dependent change of V_{DD} bias voltage. The system is therefore no longer linear time invariant (LTI). To overcome this problem, Ren and Oh [6] proposed a technique that is capable of capturing the nonlinear behavior of the driver by using 2^m bit pattern responses as the bases for superposition, where "*m*" is called the order of the method and depends on the nonlinearity of the driver. For slightly nonlinear driver, a small m would be adequate. For $m = 1$, this method is equivalent to the double step response method in [4]. With these bases, the received PRBS waveform can be directly constructed and then analyzed. Details will be given in Section II.

Apart from construction approach, there are estimation method for the worst-case eye diagram [2]–[4], [6] as well as statistical eye diagram [2], [7], [8]. In these methods, the basis waveforms such as SBR or bit pattern responses are still required in the first step. Then the final eye diagram, either worst case or statistical, is directly calculated by carefully inspecting the basis waveforms. These estimation methods, also based on the "principle" of superposition, have two advantages over the aforementioned construction approach. First, the resulting eye diagram is more accurate and reliable than the one obtained using constructing approach in the sense that all possible linear combinations of the bases are counted in these formulas. Second, the computing time of these formulas only depends on the number and the length of the bases, whereas the construction approach also depends on the length of the PRBS. If PRBS is short, say, only 1000 bits, then the construction process is fast, but the result is not highly reliable. If, on the other hand, the PRBS is sufficiently long to include all possible bases combinations, then the computing time will be much longer. The accuracy of the estimation methods, however, is completely identical to the construction approach with the same set of bases. Hence, as long as the basis waveforms are adequate to model the nonlinear behavior of the system within acceptable error, the estimation methods will provide reliable results efficiently.

For the worst eye, estimation methods based on SBR [2], step response [3], double step responses [4], and multiple pattern responses [6] have been proposed. In [6], nonlinear effects are included at the price of requiring 2^m basis waveforms. For the statistical eye, however, only the formulas for SBR [2] and double step responses [7], [8] have been proposed, whereas those for the more complicated multiple bit pattern basis remain undeveloped. Therefore, in this paper, an estimation method for calculating statistical eye diagram based on the multiple pattern scheme is proposed. Since 2^m bases are used, nonlinear effects are captured in the results. With the statistical distribution, far more information can be readily obtained, such as bit

Manuscript received February 18, 2015; revised July 2, 2015; accepted July 6, 2015. Date of publication August 14, 2015; date of current version December 11, 2015. This work was supported by the National Science Council of Taiwan under Grant NSC 101-2221-E-002-127-MY3.

The authors are with the Electrical Engineering Department, National Taiwan University, Taipei 10617, Taiwan (e-mail: tlwu@ntu.edu.tw).

Color versions of one or more of the figures in this paper are available online at http://ieeexplore.ieee.org.

Digital Object Identifier 10.1109/TEMC.2015.2457928

error rate (BER), bathtub curve, eye diagram combined with the receiver random jitter, and the worst-case eye height and jitter as well, which is just the inner boundary of the statistical eye where the probability goes to zero. Section II will introduce the mathematical background of these estimation methods. Section III generalizes the formulas to the multiple bit pattern scheme. Section IV verifies the proposed method by simulation. Section V discusses some important issues about the proposed method. Finally, a conclusion will be given.

II. Mathematical Background of Estimation Methods

Section II-A covers the basic equations of superposition technique and explains their meaning. Section II-B introduces the idea of statistical analysis and the equation based on SBR.

A. Superposition Equation

The input signal $x(t)$ of the output driver can be expressed as the superposition of the unit step function $u(t)$ in two ways

$$\begin{aligned} x(t) &= \sum_{n=0}^{\infty} (b[n] - b[n-1])u(t - nT) \\ &= \sum_{n=0}^{\infty} b[n](u(t - nT) - u(t - (n-1)T)) \end{aligned} \tag{1}$$

where $b[n]$ is the input binary signal (either 1 or 0) and T the unit interval (UI), i.e., the period of one bit. If $n < 0, b[n] = 0$. At the receiver end, the received signal $y(t)$ can be approximated as, following the second equality of (1)

$$y(t) = \sum_{n=0}^{\infty} b[n]\mathrm{SBR}(t - nT - T_d) \tag{2}$$

where T_d is the time delay of the channel and $\mathrm{SBR}(t) \equiv y^{010}(t + T + T_d)$ is the received waveform when the input is "010." In the multiple bit pattern method [6], the received signal is written as, following the first equality in (1)

$$y(t) = \sum_{n=0}^{\infty} |b[n] - b[n-1]| S^{b[n-m]\ldots b[n-1]b[n]}(t - nT - T_d) \tag{3}$$

$$\begin{aligned} S^{b_m \ldots b_1 b_0}(t) \equiv\ & y^{b_m \ldots b_1 b_0}(t + mT + T_d) \\ & - y^{b_m \ldots b_1 b_1}(t + mT + T_d) \end{aligned} \tag{4}$$

where $S(t)$ is the specific rising or falling response with m preceding bits being $b[n-m]$ to $b[n-1]$, i.e., the waveform used for superposition is dynamically selected based on the preceding bit patterns. The factor $|b[n] - b[n-1]|$ indicates that we need to superpose another basis only when there is a *transition* in the input binary signal. Example of using such bases for superposition can be found in [5]. It can be seen from the definition of $S(t)$ that the shape of $S(t)$ is either a single rising transition or a single falling transition, starting at $t = 0$. This particular rising/falling transition is the one that carries the unique response of the non-LTI system when the m preceding bits are $b[n-m]$ to $b[n-1]$. Since the nonlinear effects usually do not propagate over a very long time, by selecting m large enough presumably all the nonlinear effects in the circuit can be captured in these $S(t)$'s, at the cost of 2^m many basis waveforms. Thus, m is called the order and is a measure of the nonlinearity of the system. Conceptually, selecting a larger m not only results in a more accurate estimation but also makes the preparation work more tedious. Practically, using order 2–4 would give reasonably accurate results and the time required would be much less than PRBS method.

B. Statistical Analysis

The statistical eye, or the probability density function (PDF), proposed in [2], can be calculated recursively as

$$z_{k+1}(t, v) = \frac{\delta(v - SBR(t - (k+1)T)) + \delta(v)}{2} \otimes z_k(t, v) \tag{5}$$

where $\delta(v)$ is the delta function, $\otimes$ the convolution operator on v, and $z_k(t,v)$ the PDF with horizontal axis time, vertical axis voltage, and function value probability density. Note that the time variable $t \in [0,T)$ and the index k goes from $-N$ to -1, where N is the duration (in UI) of SBR in which $\mathrm{SBR}(t) \neq 0$. The initial condition is $z_{(-N)}(t, v) = \delta(v)$. The 1/2 factor reflects that there is an equal probability of transmitting "1" and "0." The effect of transmitting a "1" at $(-k)$ bits earlier is just to add the voltage $SBR\ (t - kT)$ at the current UI. This fact follows directly from (2). Thus, when transmitting a 1, we convolve the PDF with $\delta\ (v - \mathrm{SBR}(t - kT))$. If a "0" is transmitted, the PDF convolve with $\delta(v)$ and is unchanged, because from (2), no voltage will be added to the current UI when transmitting a "0." Thus, the PDF $z_k(t,v)$ really means the probability distribution at the current UI when the effects of (N) to $(-k)$ UI earlier transmitted signals are all considered. After running the convolution from $k = -N$ to -1, all possible intersymbol interference (ISI) effects on the current bit due to previously transmitted signals are included in the PDF. The final statistical eye is simply $z_0(t,v)$. Note that the PDF is always normalized, i.e., $\Sigma_v\{z_k(t, v)\} = 1\ \forall t$.

III. Proposed Estimation Method

Based on the multiple bit pattern superposition (3), we propose that the convolution algorithm (5) can be extended as

$$\begin{aligned} z_{k+1}^{b_m \ldots b_1}(t, v) =\ & \frac{1}{2}\delta(v - S^{0b_m \ldots b_1}(t - (k+1)T)) \otimes z_k^{0b_m \ldots b_2}(t, v) \\ & + \frac{1}{2}\delta(v - S^{1b_m \ldots b_1}(t - (k+1)T)) \otimes z_k^{1b_m \ldots b_2}(t, v) \end{aligned} \tag{6}$$

where $z_k^{b_m \ldots b_1}(t, v)$ is, as before, the PDF at the current UI when the effects of (N) to $(-k)$ UI earlier transmitted signals are considered, with the constraint that the $(-k - m + 1)$ to $(-k)$ earlier transmitted bits are exactly $b_m, \ldots, b_1$. This extra condition must be posed because, in the multibasis scheme, the waveform used for superposition is selected based on what m-bit pattern just transmitted is. For a particular m-bit pattern, $z_{k+1}^{b_m \ldots b_1}$ can be achieved by two possible ways: $z_k^{0b_m \ldots b_2}$ followed by a $b_2 b_1$ transition, and $z_k^{1b_m \ldots b_2}$ followed by a $b_2 b_1$ transition. These correspond to the two convolutions in (6). The two bases

$S(t)$ inside the delta functions are just the right ones that not only can be legally superposed after the bit pattern $0\, b_m \ldots b_2$ or $1 b_m \ldots b_2$ but also result in having the last m-bit pattern being $b_m \ldots b_1$. Thus, they are combined in the convolution to form $z_{k+1}^{b_m \ldots b_1}(t, v)$. Note that if $b_2 = b_1$, the two bases are completely zero according to (4), which means that there was no transition ($-k$) bits earlier, and thus, the PDF does not have to change. The 1/2 factor reflects that there is an equal probability of transmitting a "0" and a "1" signal. The index k goes from $-N$ to -1, where N is now the duration (in UI) of the longest basis $S(t)$ in which $|S(t)| - V_1 \neq 0$, where V_1 is the voltage difference between logic "1" and logic "0." The initial conditions are

$$z_{-N}^{b_m \ldots b_1}(t, v) = \begin{cases} \delta(v), & \text{if } b_1 = 0 \\ \delta(v - V_1), & \text{if } b_1 = 1 \end{cases}. \tag{7}$$

These initial conditions reflect that any switching—1 to 0 or 0 to 1—that happens more than N bits earlier is assumed to have no ISI effects on the current UI. Thus, the initial condition is simply a delta function at $v = 0$ or $v = V_1$.

For order m, there are total 2^m PDFs that undergo convolution concurrently. It can be easily checked that PDF $z_k^{b_m \ldots b_2 1}$ is always in the form of a distribution around $v = V_1$, for $-1 \geq k \geq -N$, while $z_k^{b_m \ldots b_2 0}$ is around $v = 0$. It is important to note that, although the voltage level of logic 0 may not be exactly 0 V, the basis waveforms $S(t)$ always start from 0 V and then rise to V_1 or fall to $-V_1$. As a result, the PDF z_k is around either V_1 or 0. We can, nevertheless, shift the final PDF to the true voltage level of logic "1" and logic "0" after the whole convolution process is done.

The final statistical distribution is obtained by adding all the $z_0(t, v)$'s together and then normalizing it. An example of a 1UI-wide eye diagram is shown in Fig. 1(a). A 2UI-wide eye diagram, if preferred, can be constructed by duplicating the 1UI eye and placing them side by side, as shown in Fig. 1(b). The reason for doing this is that the probability distribution at any UI should be completely identical, providing the probabilities of transmitting a "0" and a "1" remain constant in time. As can be seen in Fig. 1(b), the connection of the PDFs across the junction between the two UIs is indeed very smooth. Alternatively, one can properly shift the 1UI eye diagram to make the eye opening locate right at the middle of the figure, as shown in Fig. 1(c). After obtaining the statistical eye, which includes all the deterministic jitter, one can convolve it with the receiver random jitter distribution to get the eye that includes both deterministic and random jitter. We will take order 1 and order 2 as examples to demonstrate the process of (6).

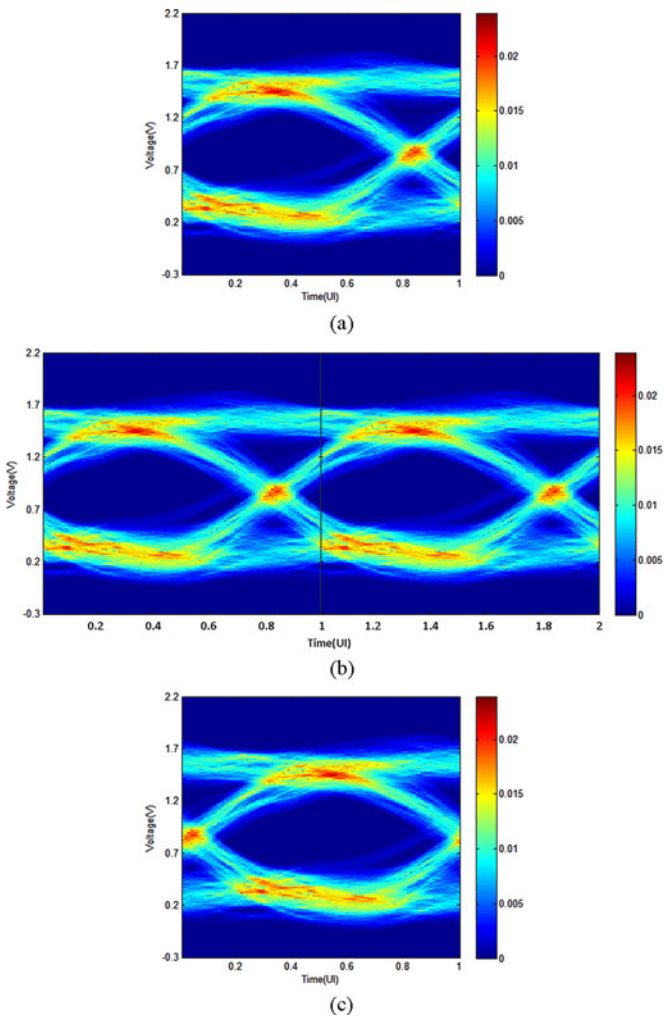

Fig. 1. (a) Example of a statistical eye diagram computed from (6). The color of each pixel represents the probability of having such voltage at such time. (b) 2UI statistical eye diagram obtained by duplicating the 1UI eye in (a). (c) 1UI eye diagram obtained by properly shifting the eye in (a).

A. Case 1: Order 1

For order 1, there are only two bases: $S^{01}(t)$ and $S^{10}(t)$, which correspond to a rising transition and a falling transition, respectively. Equation (6) reduces to

$$\begin{cases} z_{k+1}^0(t, v) = \dfrac{\delta(v)}{2} \otimes z_k^0(t, v) \\ \qquad\qquad + \dfrac{\delta(v - S^{10}(t - (k+1)T))}{2} \otimes z_k^1(t, v) \\ z_{k+1}^1(t, v) = \dfrac{\delta(v - S^{01}(t - (k+1)T))}{2} \otimes z_k^0(t, v) \\ \qquad\qquad + \dfrac{\delta(v)}{2} \otimes z_k^1(t, v) \end{cases} \tag{8}$$

with initial conditions

$$\begin{cases} z_{-N}^0(t, v) = \delta(v) \\ z_{-N}^1(t, v) = \delta(v - V_1) \end{cases} \tag{9}$$

For demonstration, assume the two bases are as in Fig. 2(a). Here, $N = 3$ by definition. Then the process of (8) is illustrated step by step as in Fig. 2(b). After three iterations, we obtain

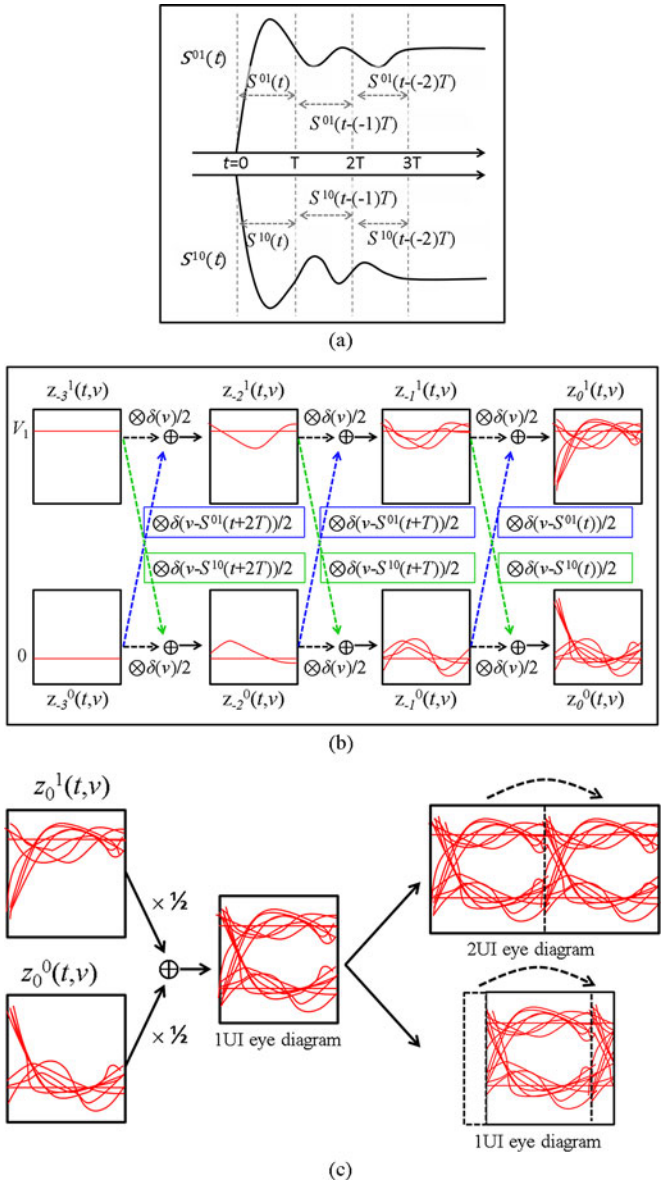

Fig. 2. (a) An example of order-1 bases: rising waveform $S^{01}(t)$ and falling waveform $S^{10}(t)$. Both waveforms are 3UI long, i.e., $N = 3$. (b) An illustration of the process (8) using the bases in (a). After three iterations of convolution, the final PDFs are obtained. (c) Adding the two $z_0(t,v)$ together results in the complete statistical eye distribution. A 2UI eye diagram or a 1UI eye located right at the middle of the figure can be obtained as shown.

$z_0^1(t,v)$ and $z_0^0(t,v)$. Here, $z_0^1(t,v)$ is the probability density (or simply probability, if the time and voltage axes are discretized) at voltage v and time t when the transmitted signal just at this UI is a "1." Likewise, $z_0^0(t,v)$ is the probability when transmitting a "0" at this UI. The complete statistical eye diagram can be constructed by simply adding $z_0^1(t,v)$ and $z_0^0(t,v)$ together and dividing each element by two, as shown in Fig. 2(c).

The order 1 formulation (8) can be shown to be mathematically equivalent to the estimation method in [7] and [8], but the basis waveforms used are quite different. In this paper, the bases are defined based on the concept of multiple pattern responses as in (4) and can be easily generalized to higher order cases.

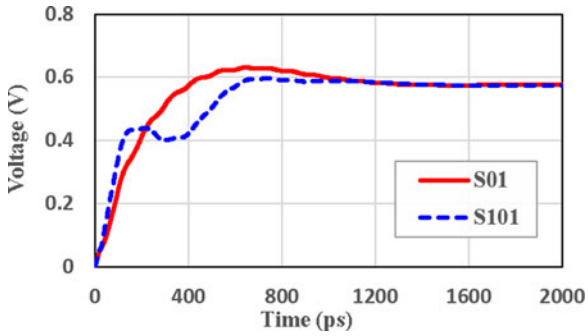

Fig. 3. Comparison of the bases $S^{001}(t)$ and $S^{101}(t)$.

B. Case 2: Order 2

There are four bases for order 2: $S^{001}(t)$ and $S^{101}(t)$, which are rising transitions, and $S^{110}(t)$ and $S^{010}(t)$, which are falling transitions. An example of $S^{001}(t)$ and $S^{101}(t)$ is shown in Fig. 3, from which a clear difference between them can be observed. For channels like this, errors will occur if one uses only order 1 bases to predict the eye diagram because in order-1 scheme, the rising transition $S^{101}(t)$ is assumed to be the same as $S^{001}(t)$. This is why order 2 or higher order bases and their corresponding estimation formulas are needed.

There are four PDFs for order 2. The formula (6) becomes

$$\begin{cases} z_{k+1}^{00}(t,v) = \dfrac{\delta(v)}{2} \otimes z_k^{00}(t,v) + \dfrac{\delta(v)}{2} \otimes z_k^{10}(t,v) \\ z_{k+1}^{01}(t,v) = \dfrac{\delta(v - S^{001}(t-(k+1)T))}{2} \otimes z_k^{00}(t,v) \\ \qquad\qquad + \dfrac{\delta(v - S^{101}(t-(k+1)T))}{2} \otimes z_k^{10}(t,v) \\ z_{k+1}^{10}(t,v) = \dfrac{\delta(v - S^{010}(t-(k+1)T))}{2} \otimes z_k^{01}(t,v) \\ \qquad\qquad + \dfrac{\delta(v - S^{110}(t-(k+1)T))}{2} \otimes z_k^{11}(t,v) \\ z_{k+1}^{11}(t,v) = \dfrac{\delta(v)}{2} \otimes z_k^{11}(t,v) + \dfrac{\delta(v)}{2} \otimes z_k^{01}(t,v) \end{cases} \tag{10}$$

The initial conditions are

$$\begin{cases} z_{-N}^{00}(t,v) = z_{-N}^{10}(t,v) = \delta(v) \\ z_{-N}^{01}(t,v) = z_{-N}^{11}(t,v) = \delta(v - V_1) \end{cases} \tag{11}$$

The process of (10) is illustrated in Fig. 4. Here, $z_0^{b_2 b_1}(t,v)$ is the probability distribution when the transmitted signal is b_1 right at the current UI and b_2 at the previous UI. As before, adding the four PDFs $z_0^{00}(t,v)$, $z_0^{01}(t,v)$, $z_0^{10}(t,v)$, and $z_0^{11}(t,v)$ together and dividing it by 4 result in the final statistical eye diagram.

C. PDF of Specific Signal Pattern

The 2^m final PDFs $z_0^{b_m \cdots b_1}(t,v)$ contain a lot of information. Suppose the 2UI PDF in which the transmitted signal at the first UI is "1" is required. We could synthesize it using $z_0^{b_m \cdots b_1}(t,v)$

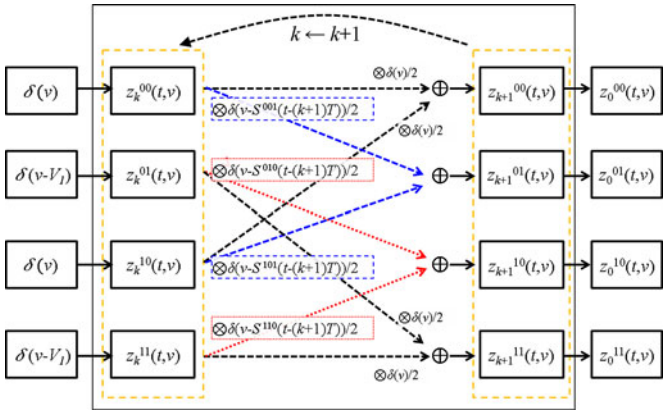

Fig. 4. Update process of (10). There are four PDFs and four bases for order 2.

as, assuming order $m \geq 2$

$$\mathrm{PDF}_1^1(t,v) = \sum_{\substack{\text{all possible} \\ b_{m-1},\ldots,b_1}} \frac{1}{2^{m-1}} z_0^{b_{m-1}\ldots b_2 b_1 1}(t,v)$$

$$\mathrm{PDF}_2^1(t,v) = \sum_{\substack{\text{all possible} \\ b_{m-1},\ldots,b_1}} \frac{1}{2^{m-1}} z_0^{b_{m-1}\ldots b_2 1 b_1}(t,v) \quad (12)$$

where $\mathrm{PDF}_1{}^1(t,v)$ and $\mathrm{PDF}_2{}^1(t,v)$ are the PDFs of the first and second UI, respectively. The $1/2^{(m-1)}$ factors are for normalization. Likewise, the 2UI PDF in which the first UI is transmitting a "0" can be constructed using (12) with $z_0^{b_{m-1}\ldots b_2 b_1 1}$ and $z_0^{b_{m-1}\ldots b_2 1 b_1}$ replaced by $z_0^{b_{m-1}\ldots b_2 b_1 0}$ and $z_0^{b_{m-1}\ldots b_2 0 b_1}$, respectively. An example for order 2 is shown in Fig. 5, in which (a) represents first bit "1" case and (b) represents first bit "0" case. For (a), $PDF_1^1(t,v) = (z_0^{01}(t,v) + z_0^{11}(t,v))/2$. $PDF_2^1(t,v) = (z_0^{10}(t,v) + z_0^{11}(t,v))/2$. For (b), $PDF_1^0(t,v) = (z_0^{00}(t,v) + z_0^{10}(t,v))/2$. $PDF_2^0(t,v) = (z_0^{00}(t,v) + z_0^{01}(t,v))/2$.

The formula mentioned earlier is suitable for order $m \geq 2$. For $m = 1$, we also need $z_{-1}^1(t,v)$ and $z_{-1}^0(t,v)$, which are byproducts of the convolution process (8). For the first bit "1" case, $\mathrm{PDF}_1{}^1(t,v) = z_0{}^1(t,v)$, and $PDF_2^1(t,v) = 1/2(z_{-1}^1(t,v) + z_{-1}^1(t,v) \otimes \delta(v - S^{10}(t)))$. For the first bit "0" case, $PDF_1^0(t,v) = z_0^0(t,v)$, and $PDF_2^0(t,v) = 1/2(z_{-1}^0(t,v) + z_{-1}^0(t,v) \otimes \delta(v - S^{01}(t)))$. The reason is simple: Since $z_{-1}{}^b(t,v)$ is the PDF at the *current* UI with the signal of *previous* UI being "b" and all earlier ISI effects considered, the PDF at the *next* UI with the signal at the *current* UI being "b" and all the ISI effects up to the *current* UI considered, is also $z_{-1}{}^b(t,v)$. In addition, there is either no transition or a $b\bar{b}$ transition at the *next* UI. As a result, PDF_2 is calculated as mentioned earlier. A final 2UI PDF similar to Fig. 5 can be obtained. If a specific 3UI PDF is required, we need additional PDFs $z_{-2}^1(t,v)$, $z_{-2}^0(t,v)$ for order 1 and $z_{-1}{}^{00}(t,v)$, $z_{-1}{}^{01}(t,v)$, $z_{-1}{}^{10}(t,v)$, $z_{-1}{}^{11}(t,v)$ for order 2. The construction formulas are similar to the ones mentioned earlier.

Having a 2UI PDF as in Fig. 5, we can calculate the BER of transmitting "1," denoted as BER_1, and the BER of transmitting

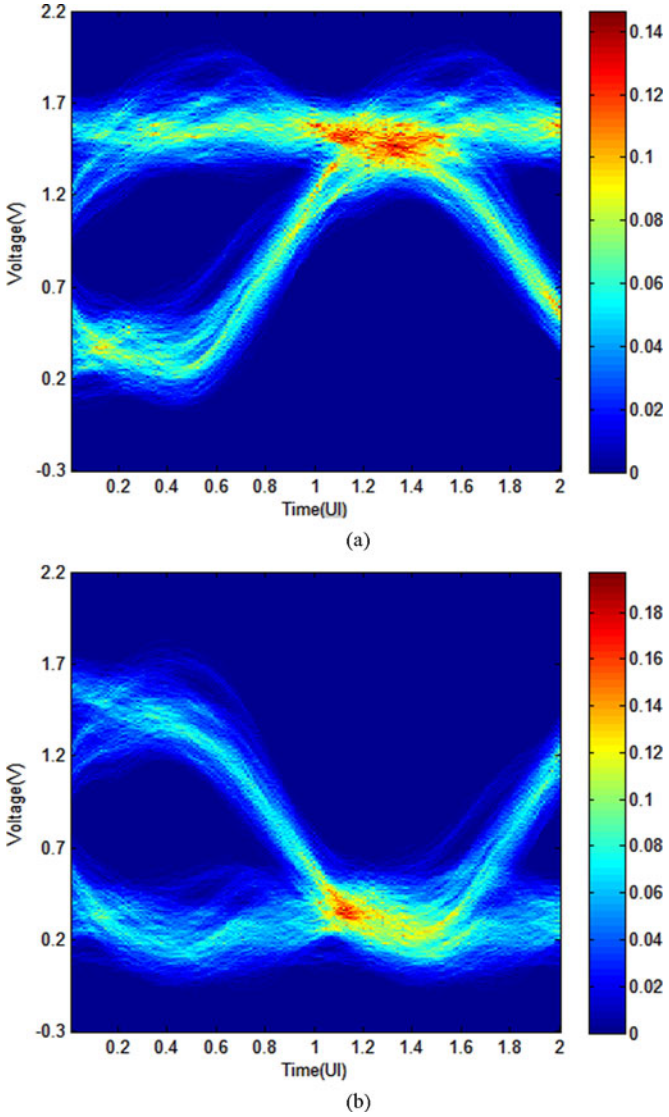

Fig. 5. (a) 2UI PDF with the first UI transmitting "1." (b) 2UI PDF with the first UI transmitting "0."

"0," denoted as BER_0, as

$$\mathrm{BER}_1(t) = \begin{cases} \sum_{v<v_t} \mathrm{PDF}_1^1(t,v), & t < T \\ \sum_{v<v_t} \mathrm{PDF}_2^1(t-T,v), & t > T \end{cases}$$

$$\mathrm{BER}_0(t) = \begin{cases} \sum_{v>v_t} \mathrm{PDF}_1^0(t,v), & t < T \\ \sum_{v>v_t} \mathrm{PDF}_2^0(t-T,v), & t > T \end{cases} \quad (13)$$

where v_t is the threshold voltage and $t \in [0, 2T)$. In other words, BER_1 is the total probability in PDF^1 at a specific sampling time t with voltage smaller than v_t, and BER_0 is the total probability in PDF^0 at sampling time t with voltage greater than v_t. The total BER can be calculated as $\mathrm{BER}(t) = \mathrm{BER}_1(t) + \mathrm{BER}_0(t)$, from which the bathtub curve can be drawn. This serves as an alternative way of obtaining the bathtub curve.

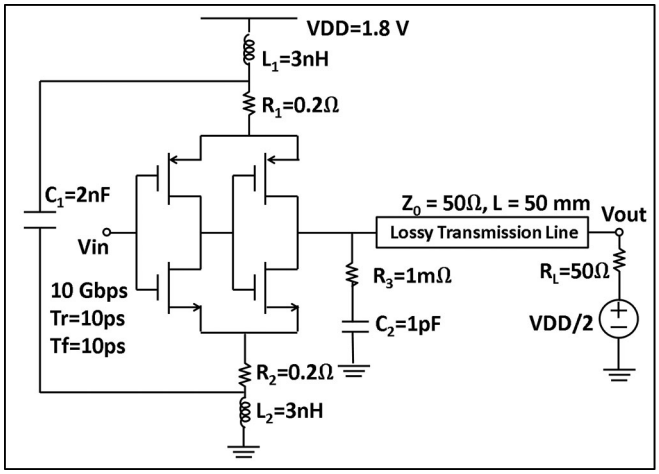

Fig. 6. Push–pull driver used for simulation.

IV. Simulation Results

Two types of circuits are used to verify the proposed method: the push–pull driver and the open-drain driver, both are CMOS 90 nm process model. Here only package level PDN is included with no board-level decoupling capacitor in order to make the nonlinear effects more pronounced. The final PDF, eye width, bathtub curve, and CPU time of each method are compared.

A. Push–Pull Driver

The topology of the push–pull driver used in simulation is shown in Fig. 6. As the name implies, a push–pull driver provides a current path to high voltage and a current path to ground. This type of driver can operate at high bit rates because the PMOS and NMOS provide a fast switch for charging and discharging. The two paths of charging and discharging, however, result in more power consumption during operation, compared with open-drain topology.

PDFs obtained from different methods are shown in Fig. 7, including SBR, proposed method with order 1–4, and 2^{13} bit PRBS. The time axis is 1 ps/div. The voltage axis is 0.1 mV/div during algorithm computation. After the algorithm process is completed, the final PDF is merged to 1 mV/div for averaging, in order to reduce possible numerical errors in SPICE.

Quantitatively, the differences between the PDFs obtained from various orders and the PDF of PRBS simulation are calculated using the measure

$$\text{Difference} = \sum_{t,v} |\text{PDF}_{method1}(t,v) - \text{PDF}_{method2}(t,v)| \tag{14}$$

which is the sum of the absolute value of the PDF difference at each cell. The results are listed in the second column of Table I. As can be seen from the table, the PDF difference becomes smaller as the order increases, which indicates that higher order results are closer to the PRBS's result. The absolute values of PDF difference, however, may not have a precise meaning. It is not easy to say that a PDF difference of 30.55 is large or small.

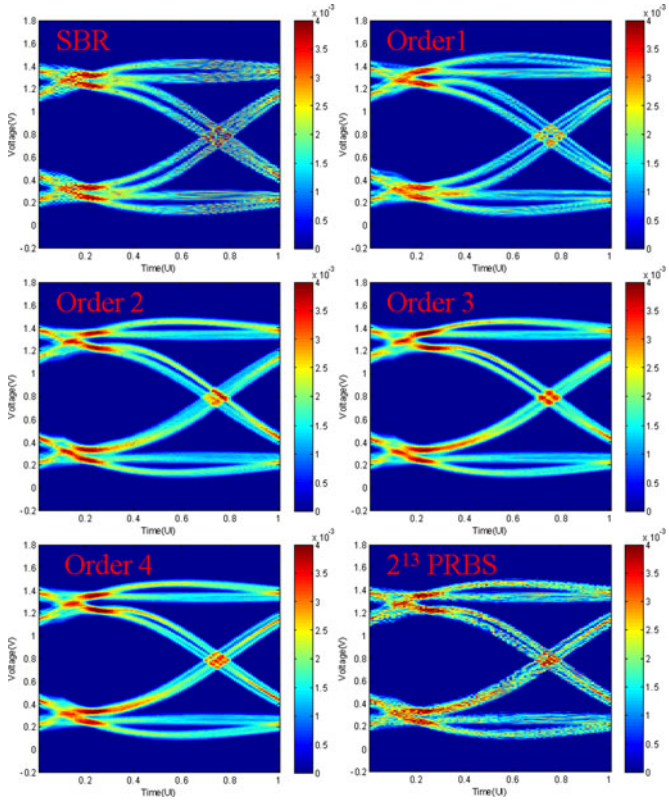

Fig. 7. PDFs obtained from different methods.

TABLE I
Comparison Between Different Methods

	Difference [using (14)]	10^{-5} Eye Width	Eye Width Error	CPU Time (s)
SBR	59.4567	0.85 UI	−2.3%	0.85
Order 1	50.1274	0.83 UI	−4.6%	0.91
Order 2	30.5542	0.85 UI	−2.3%	1.39
Order 3	28.5402	0.86 UI	−1.1%	2.35
Order 4	26.2142	0.86 UI	−1.1%	4.39
2^{13} PRBS	–	0.87 UI	–	380.7

In Table I, the BER $< 10^{-5}$ eye width, eye width error (compared with PRBS), and CPU time of each case are also shown. The eye widths of all cases are smaller than the eye width of PRBS, but there is only 1 ps difference both for orders 3 and 4, which is the minimum time step used in SPICE. Thus, the eye widths of orders 3 and 4 are actually quite accurate. The CPU times of all cases, as can be seen, are much smaller than the CPU time of PRBS simulation, which verifies the efficiency of this method. The bathtub curve of each method is shown in Fig. 8. Despite the innermost 1 ps eye width error, the overall bathtub curves of orders 3 and 4 are very close to that of PRBS.

Overall, the nonlinear behavior of this push–pull circuit is not so significant. As a result, the PDF and eye width estimations of orders 3 and 4 are reasonably accurate. This can also be seen from the basis waveforms of different orders. Some are plotted in Fig. 9. $S^{101}(t)$, which is order 2 basis as shown in Fig. 9(a), is quite different from $S^{01}(t)$, while $S^{1001}(t)$, $S^{10001}(t)$, and

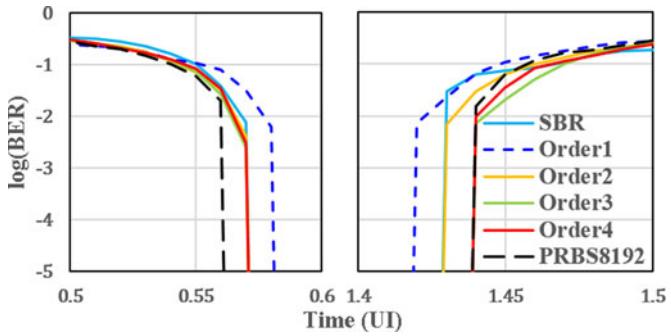

Fig. 8. Bathtub curves obtained using SBR, orders 1–4, and 8192-bit PRBS.

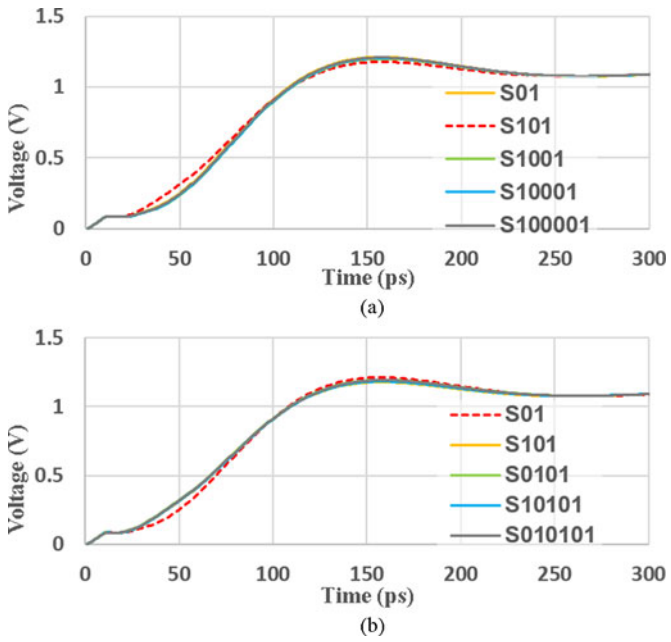

Fig. 9. Comparison of basis waveforms of different orders of the push–pull driver in Fig. 6.

$S^{100001}(t)$, which are order 3, 4, and 5 bases, do not differ significantly from $S^{01}(t)$. Similar phenomenon is observed in Fig. 9(b), in which the order 3, 4 bases $S^{0101}(t)$ and $S^{10101}(t)$ almost overlap the order 2 basis $S^{101}(t)$. These results indicate that using order 3 bases would be adequate to capture most nonlinear effects in this push–pull driver.

B. Open-Drain Driver

Open-drain driver is another topology that is commonly used in circuit design. Open-drain driver replaces the PMOS of a push–pull driver with a pull-up resistor. The channel setup is shown in Fig. 10. The replacement of the pull-up resistor may limit the maximum data rate, but it allows the receiver IC to have a different V_{DD} voltage.

The PDFs and bathtub curves of various methods, including SBR, order 1–5, and 2^{13}-bit PRBS are plotted in Fig. 11. Again, the time axis is 1 ps/div, while the voltage axis is 0.1 mV/div during algorithm computation and merged to 1 mV/div after the

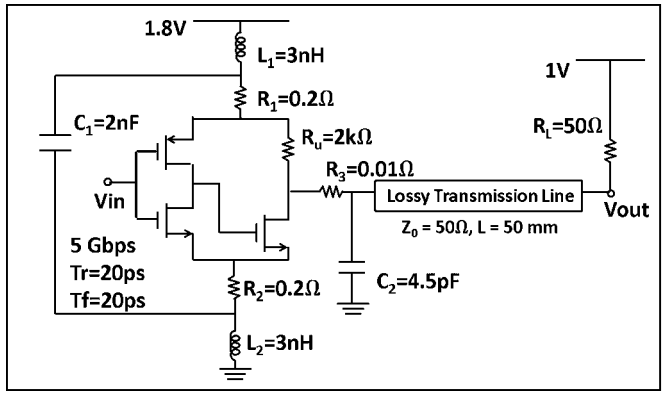

Fig. 10. Open-drain driver used for simulation.

TABLE II
COMPARISON BETWEEN DIFFERENT METHODS

Method	Difference [Using (14)]	10^{-5} Eye Width	Eye Width Error	CPU Time (s)
SBR	125.7937	0.550 UI	−11.3%	0.83
Order 1	114.4328	0.465 UI	−25.0%	1.21
Order 2	86.1790	0.305 UI	−50.8%	1.97
Order 3	69.8080	0.370 UI	−40.3%	3.50
Order 4	48.6141	0.500 UI	−19.4%	6.65
Order 5	41.0283	0.530 UI	−14.5%	12.74
2^{13} PRBS	–	0.620 UI	–	612

convolution process is completed. Unlike the push–pull driver, the open-drain driver is relatively nonlinear; thus, the predicted PDFs are not similar to that of PRBS until orders 4 and 5. The PDFs of SBR, orders 1, 2, and even 3, are all quite different from the PDFs of PRBS. In particular, the PDF of SBR has a "small-hill" at the upper half eye, which is not found in other methods. This abnormal projection is a direct consequence of using SBR superposition in an unbalanced rise/fall time channel. The detailed phenomenon has been discussed in [4]. The PDFs of orders 1, 2, and 3, although resemble the PDF of PRBS much better than SBR, still have noticeable difference. Especially, the eye openings of orders 1–3 are all significantly smaller than that of PRBS. The PDFs of orders 4 and 5, evidently, are much similar to the PDF of PRBS.

Direct comparison of PDFs using the measure (14) is listed in Table II. The difference of PDFs goes down as the order increases, which means that predicted PDFs of higher orders are more and more similar to the PDF of PRBS. Because the open-drain driver is much more nonlinear than push–pull driver, we may need order 5 or even higher order bases to accurately predict the PDF.

By looking at the eye widths in Table II and the bathtub curves in Fig. 11(b), we find that the eye width of SBR is closer to the eye width of PRBS than orders 1–5. Regarding the bizarre appearance of the PDF of SBR, however, we consider this most-accurate eye width prediction not reliable. Because the bathtub curve and thus the eye width are computed based on the PDF, the bathtub curve and the eye width of a large-error PDF are by no means trustworthy.

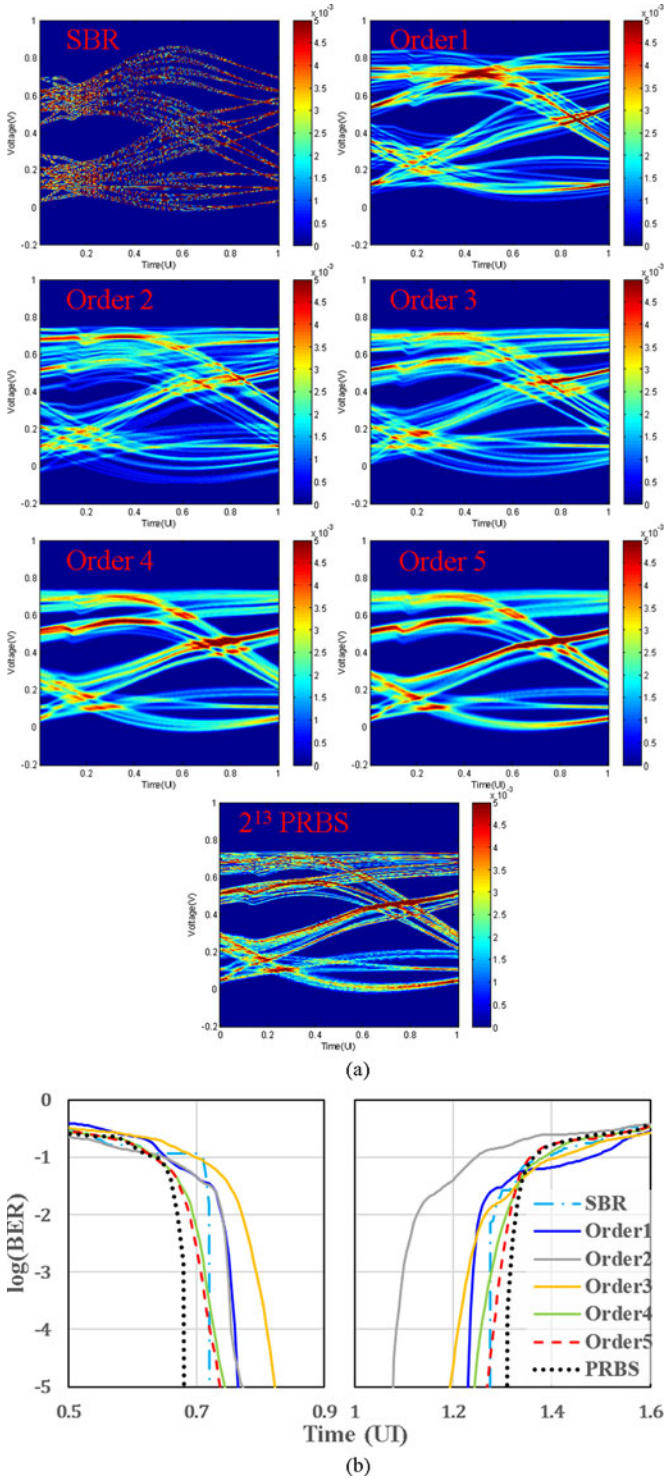

Fig. 11. (a) PDFs and (b) bathtub curves of SBR, orders 1–5, and PRBS.

Also, note that the order 2 eye width has a larger error than order 1, in contrast to the decreasing error of PDF difference. This is because, although the order 2 PDF difference is smaller than order 1, it is still large compared with orders 3–5. A large error PDF certainly does not guarantee a small error eye width. On the other hand, by looking at the basis waveforms in Fig. 12, we know that all the results of order 1–3 will not be so reliable,

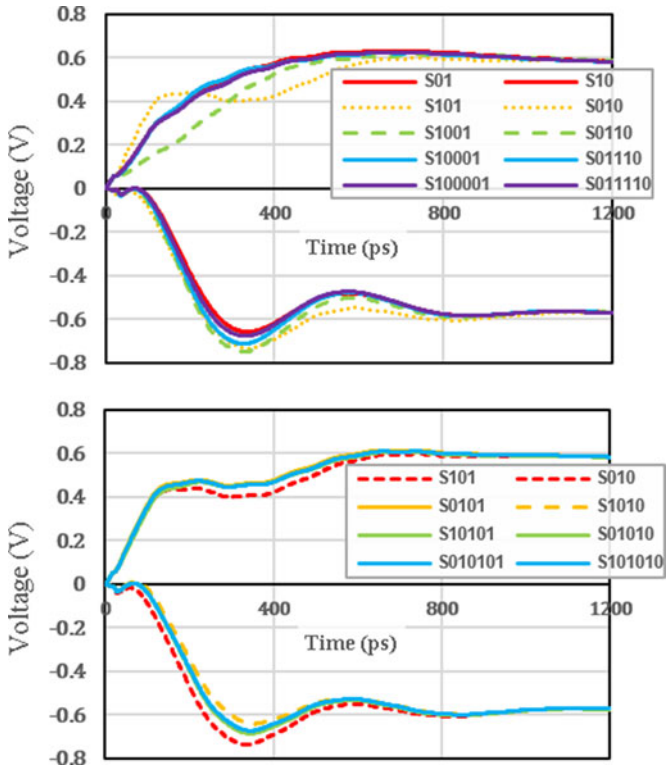

Fig. 12. Comparison of basis waveforms of different orders of the open-drain driver in Fig. 10.

and thus, the larger error of order 2 eye width does not have any significance. In Fig. 12, clearly, the order 2 and 3 bases $S^{101}(t)$ and $S^{1001}(t)$ both differ significantly from $S^{01}(t)$, and the order 3 and 4 bases $S^{1010}(t)$ and $S^{01010}(t)$ differ significantly from $S^{010}(t)$. The order 5 bases $S^{100001}(t)$, $S^{011110}(t)$, and $S^{101010}(t)$, in contrast, largely overlap the order 1 bases $S^{01}(t)$ and $S^{10}(t)$ and order 4 basis $S^{01010}(t)$, respectively, which indicates that the remaining nonlinear effect that is not captured in these order 5 bases is relatively rare. Thus, by looking at the basis waveforms, we know that at least order 5 bases should be used to characterize this open-drain circuit, and this also explains why the predicted PDFs of SBR and orders 1–3 are all considerably different from the PRBS's result. A quantitative way of evaluating the difference of bases can be found in [5].

The bathtub curves in Fig. 11(b) are calculated using the conventional jitter CDF method. It is worth comparing the bathtub curves with the ones obtained from the proposed methods (12) and (13), as shown in Fig. 13. Clearly, the proposed method gives almost identical bathtub curves compared with the conventional method, which verifies the validity of the proposed method.

To sum up, two different drivers are used to test the proposed PDF-estimation method described in Section III and the bundled bathtub curve computing method in Section III-C. The push–pull driver is quite linear and requires only order 3 bases to estimate the PDF. The open-drain driver is relatively nonlinear and requires order 5 or higher bases to accurately predict the PDF. The divergence between the predicted PDFs and the PDF of PRBS becomes smaller as the order increases. The overall

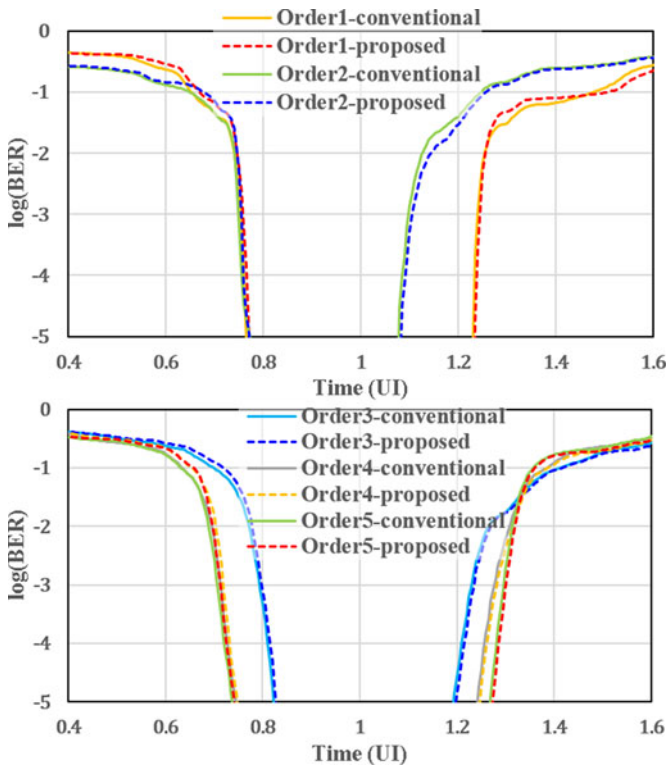

Fig. 13. Comparison of bathtub curves obtained using the conventional jitter CDF method and the proposed methods (12) and (13).

shapes of PDFs and bathtub curves of higher orders are within acceptable errors compared with PRBS. The required order can be roughly determined by comparing the difference between the basis waveforms of different orders. The bathtub curves obtained from the proposed method are in good agreement with the conventional jitter CDF method. The CPU times of the proposed algorithm for orders 1–5 are all much smaller than PRBS, which verifies the efficiency of this algorithm.

V. Discussion

Several important issues about the proposed method are discussed in this section, including the application, limitation, and accuracy of the method.

A. Application of the Method

The proposed method is for SI evaluation mainly at the *design* stage, during which only models (of circuit and package) are available. With these models at hand, engineers may try running the proposed method with order 3 or 4 to see the resulting eye diagram, instead of directly running PRBS, which takes much more time. Therefore, the proposed method is verified in this paper only via simulation but not experiment.

B. Limitation of the Method

The multiple basis scheme only captures deterministic noise. For random noise, only the receiver random jitter can be combined into the final PDF via simple convolution as, for example, see [9, Eq. (5)]. The influence of transmitter random jitter remains a difficult task. In addition to transmitter random jitter, sinusoidal jitter, duty cycle distortion, clocking scheme nonlinear effects, and channel coding are also not incorporated into the proposed method. Only when these effects are insignificant that designers can use the proposed method confidently.

C. Accuracy of the Method

The accuracy of the proposed method is closely related to the accuracy of the bases used. If the bases are accurate and capture most possible responses of the channel, then the proposed method would also be accurate. The accuracy of the bases has been investigated in [5] and [6] for some specific channels. Further study is required. In addition to the number of basis, the fidelity of the basis waveforms is another important issue. Since all possible combinations of the bases are counted in (6), tiny but long-lasting fluctuations of the basis waveform stemmed from SPICE instability will be accumulated, resulting in an unrealistically small eye opening. To solve this problem, one could truncate the basis waveform after it has reached $\pm V_1$ within certain range of tolerance.

VI. Conclusion

An estimation method for statistical eye diagram based on superposition of multiple bit pattern responses was proposed. The method captured the nonlinear effects of the channel by using 2^m bases. The method was time-saving compared with PRBS simulation. Further extension of this method to include transmitter random jitter, sinusoidal jitter, and duty cycle distortion is an important future work.

References

[1] T. L. Wu, F. Buesink, and F. Canavero, "Overview of signal integrity and EMC design technologies on PCB: Fundamentals and latest progress," *IEEE Trans. Electromag. Compat.*, vol. 55, no. 4, pp. 624–638, Aug. 2013.

[2] B. K. Casper, M. Haycock, and R. Mooney "An accurate and efficient analysis method for multi-Gb/s chip-to-chip signaling schemes," in *Symp. VLSI Circuits Dig. Tech. Papers*, Jun. 2002, pp. 54–57.

[3] Y. C. Lai, "Fast eye diagram algorithm and FIR compensation design for general transmission line systems," M.S. thesis, Dept. Elect. Eng., National Taiwan Univ., Taipei, Taiwan, 2010.

[4] R. Shi, W. Yu, Y. Zhu, C.K. Cheng, and E. S. Kuh, "Efficient and accurate eye diagram prediction for high speed signaling," in *Proc. IEEE/ACM ICCAD*, Nov. 2008, pp. 655–661.

[5] C. C. Chou, H. H. Chuang, T. L. Wu, S. H. Weng, and C. K. Cheng "Eye prediction of digital driver with power distribution network noise," in *Proc. IEEE EPEPS*, Oct. 2012, pp. 131–134.

[6] J. Ren and D. Oh, "Multiple edge responses for fast and accurate system simulations," *IEEE Trans. Adv. Packag.*, vol. 31, no. 4, pp. 741–748, Nov. 2008.

[7] B. Casper, G. Balamurugan, J. E. Jaussi, J. Kennedy, and M. Mansuri, "Future microprocessor interfaces: Analysis, design and optimization," in *Proc. IEEE CICC*, Sep. 2007, pp. 479–486.

[8] A. Cristofoli, P. Palestri, N. Da Dalt, L. Selmi, "Efficient statistical simulation of intersymbol interference and jitter in high-speed serial interfaces," *IEEE Trans. Compon., Packag. Manuf. Technol.*, vol. 4, no. 3, pp. 480–489, Mar. 2014.

[9] Z. Chen, W. D. Becker, and G. Katopis, "A new approach to deriving packaging system statistical eye diagram based on parallel non-linear transient simulations using multiple short signal bit patterns," in *Proc. ECTC*, May 2012, pp. 160–167.

[10] V. Stojanovic and M. Horowitz, "Modeling and analysis of highspeed links," in *Proc. IEEE Custom Integr. Circuits Conf.*, Sep. 2003, pp. 589–594.
[11] G. Balamurugan, B. Casper, J. E. Jaussi, M. Mansuri, F. O'Mahony, and J. Kennedy, "Modeling and analysis of high-speed I/O links," *IEEE Trans. Adv. Packag.*, vol. 32, no. 2, pp. 237–247, May 2009.
[12] B. Analui, J. Buckwalter, and A. Hajimiri, "Data-dependent jitter in serial communications," *IEEE Trans. Microw. Theory Tech.*, vol. 53, no. 11, pp. 1841–1844, Nov. 2005.
[13] K. S. Oh, F. Lambrecht, S. Chang, Q. Lin, J. Ren, C. Yuan, J. Zerbe, and V. Stojanovic, "Accurate system voltage and timing margin simulation in high-speed I/O system designs," *IEEE Trans. Adv. Packag.*, vol. 31, no. 4, pp. 722–730, Nov. 2008.
[14] D. Oh, J. Ren, and S. Chang, "Hybrid statistical link simulation technique," *IEEE Trans. Compon. Packag. Manuf. Technol.*, vol. 1, no. 5, pp. 772–783, May 2011.
[15] P. K. Hanumolu, B. Casper, R. Mooney, G. Y. Wei, and U. K. Moon, "Analysis of PLL clock jitter in high speed serial links," *IEEE Trans. Circuits Syst. II Analog Digit. Signal Process.*, vol. 50, no. 11, pp. 879–886, Nov. 2003.
[16] J. Buckwalter, B. Analui, and A. Hajimiri, "Predicting data-dependent jitter," *IEEE Trans. Circuits Syst. II Tech. Briefs*, vol. 51, no. 9, pp. 453–457, Sep. 2004.
[17] G. Kim, D. G. Kam, S. J. Lee, J. Kim, M. Ha, K. Koo, J. S. Pak, and J. Kim, "Modeling of eye-diagram distortion and data-dependent jitter in meander delay lines on high-speed printed circuit boards (PCBs) based on a time-domain even-mode and odd-mode analysis," *IEEE Trans. Microw. Theory Tech.*, vol. 56, no. 8, pp. 1962–1972, Aug. 2008.
[18] K. Xiao, B. Lee, and X. Ye, "A flexible and efficient bit error rate simulation method for high-speed differential link analysis using time-domain interpolation and superposition," in *Proc. IEEE Int. Symp. Electromagn. Compat.*, Aug. 2008, pp. 1–6.
[19] D. Oh, S. Chang, J. Ren, L. Yang, H. Lan, C. Madden, and R. Schmitt, "Statistical link analysis and in-situ characterization of high-speed memory bus in 3D package systems," in *Proc. IEEE Int. Symp. Electromagn. Compat.*, Aug. 2011, pp. 797–802.

Chiu-Chih Chou received the B.S.E.E. degree in 2011 from National Taiwan University (NTU), Taipei, Taiwan, where he is currently working Ph.D. degree at the Graduate Institute of Communication Engineering.

His current research interests include EMC/EMI and signal integrity design for high-speed digital systems.

Sheng-Yun Hsu received the B.S.E.E. degree from the National Central University, Taoyuan, Taiwan, in 2012, and the Master's degree from the Graduate Institute of Communication Engineering, National Taiwan University, Taipei, Taiwan, in 2014.

His current research interests include signal integrity and EMC design.

Tzong-Lin Wu (S'93–M'98–SM'04–F'13) received the B.S.E.E. and Ph.D. degrees from National Taiwan University (NTU), Taipei, Taiwan, in 1991 and 1995, respectively.

From 1995 to 1996, he was a Senior Engineer at Micro-electronics Technology Inc., Hsinchu, Taiwan. In 1996, he joined the Central Research Institute of the Tatung Company, Taipei, Taiwan, where he was involved in the analysis and measurement of electromagnetic compatibility/electromagnetic interference (EMC/EMI) problems of high-speed digital systems. In 1998, he decided in favor of an academic career and accepted a position in the Electrical Engineering Department, National Sun Yat-Sen University. Since 2006, he has been a Professor in the Department of Electrical Engineering, Graduate Institute of Communication Engineering (GICE), NTU. His current research interests include EMC/EMI and signal/power integrity design for high-speed digital/optical systems. He was appointed as the Director of the GICE and Communication Research Center, NTU, in 2012. The research direction of GICE includes EM wave, communication, and multimedia.

Dr. Wu received the Excellent Research Award and the Excellent Advisor Award from National Sun Yat-Sen University in 2000 and 2003, respectively, the Outstanding Young Engineers Award from the Chinese Institute of Electrical Engineers in 2002, and the Wu Ta-You Memorial Award from the National Science Council (NSC) in 2005, the Outstanding Research Award from NSC in 2010 and 2014, and the IEEE Transactions on Advanced Packaging Best Paper Award in 2011. He has served as the Chair of the Institute of Electronics, Information, and Communication Engineers (IEICE) Taipei Section in 2007–2011, the Treasurer of the IEEE Taipei Section in 2007–2008, and was a member of the Board of Directors of the IEEE Taipei Section in 2009–2010 and 2013–2016. He was the IEEE EMC Society as a Distinguished Lecturer for the period 2008–2009. He was the Co-Chair of the 2007 IEEE Electrical Design of Advanced Packaging and Systems (EDAPS) workshop, the General Chair of the 2015 Asia Pacific EMC Symposium (APEMC), and the Technical Program Chair of the 2010 and 2012 IEEE EDAPS Symposiums. He is now the Associate Editor of the IEEE TRANSACTIONS ON ELECTROMAGNETIC COMPATIBILITY and the IEEE TRANSACTIONS ON COMPONENTS, PACKAGING, AND MANUFACTURING TECHNOLOGIES.